

In vitro and in vivo degradation evaluation of novel iron- bioceramic composites

by A Kafrawi Nasution

Submission date: 17-Nov-2020 04:16PM (UTC+0800)

Submission ID: 1448797317

File name: vel_iron-bioceramic_composites_for_bone_implant_applications.pdf (1.84M)

Word count: 6265

Character count: 32311



Contents lists available at ScienceDirect

Materials Science and Engineering C

journal homepage: www.elsevier.com/locate/msec

In vitro and *in vivo* degradation evaluation of novel iron-bioceramic composites for bone implant applications

M.F. Ulum^{a,b}, A. Arafat^{a,c,1}, D. Noviana^b, A.H. Yusop^a, A.K. Nasution^{a,d}, M.R. Abdul Kadir^a, H. Hermawan^{a,*}^a Faculty of Biosciences and Medical Engineering, Universiti Teknologi Malaysia, Johor Bahru, Malaysia^b Faculty of Veterinary Medicine, Bogor Agricultural University, Bogor, Indonesia^c Faculty of Mechanical Engineering, Universiti Teknologi Malaysia, Johor Bahru, Malaysia^d Faculty of Engineering, Muhammadiyah University of Riau, Pekanbaru, Indonesia

ARTICLE INFO

Article history:

Received 27 May 2013

Received in revised form 6 November 2013

Accepted 17 December 2013

Available online 26 December 2013

Keywords:

Biodegradable metals

Iron

Bioceramics

Degradation

Cytotoxicity

Implantation

ABSTRACT

Biodegradable metals such as magnesium, iron and their alloys have been known as potential materials for temporary medical implants. However, most of the studies on biodegradable metals have been focusing on optimizing their mechanical properties and degradation behavior with no emphasis on improving their bioactivity behavior. We therefore investigated the possibility of improving iron biodegradation rate and bioactivity by incorporating various bioactive bioceramics. The iron-based bioceramic (hydroxyapatite, tricalcium phosphate and biphasic calcium phosphate) composites were prepared by mechanical mixing and sintering process. Degradation studies indicated that the addition of bioceramics lowered the corrosion potential of the composites and slightly increased their corrosion rate compared to that of pure iron. *In vitro* cytotoxicity results showed an increase of cellular activity when rat smooth muscle cells interacted with the degrading composites compared to pure iron. X-ray radiogram analysis showed a consistent degradation progress with that found *in vivo* and positive tissue response up to 70 days implantation in sheep animal model. Therefore, the iron-based bioceramic composites have the potential to be used for biodegradable bone implant applications.

© 2013 Elsevier B.V. All rights reserved.

1. Introduction

Recent progress in the biomedical field can be attributed to better understanding bioactive materials which have the ability to promote positive interactions with the physiological environment. In certain cases, biomaterials are only needed temporarily to support the healing process and are expected to degrade thereafter [1,2]. In orthopedic applications, biodegradable implants should allow a gradual load transfer to the healing bone as the materials degrade, thus reducing the stress shielding phenomenon. It also eliminates a secondary operation to remove the implant which is common with non-degradable metallic implants [3–5]. Magnesium (Mg)- and iron (Fe)-based alloys are two classes of metals which have received attention for temporary implant applications such as bone pins, plates, screws and stents [6–8]. Most of the studies on Mg and its alloys reported a rapid degradation rate in physiological environments [9,10], while the degradation rates of Fe and its alloys were considered too slow [11,12]. Alloying Fe with other elements such as Mn, C, Si, and Pd improved its degradation rate, but their biocompatibility is uncertain at higher concentrations of the alloying elements [13–17]. An alternative approach is needed to develop Fe-based material with improved degradation behavior while maintaining its biocompatibility.

Calcium phosphate ceramics, such as hydroxyapatite (HA), tricalcium phosphate (TCP) and biphasic calcium phosphate (BCP) are known bioceramics with bioactivity that supports cell proliferation, bone ingrowth and osseointegration. These bioceramics have been widely used in orthopedics and dentistry [18,19]. Their main components, Ca and P, are both essential elements that maintain physiological homeostasis processes with balanced cell proportions [20]. These bioactive ceramics are also degradable with different solubility in body environment, and can be controlled by manipulating the composition (HA/TCP ratio) [21]. These characteristics, when incorporated into biodegradable metals where an improvement to both their degradation and bioactivity is expected, are appealing. Therefore, this work aims to develop novel biodegradable materials by incorporating HA, TCP and BCP into Fe to form Fe-bioceramic composites. These composites are the first of its kind in the field of biodegradable material for temporary implants. The mechanical behavior and degradation rate were studied, and their *in vitro* cytotoxicity was evaluated via direct and indirect contact with rat smooth muscle cells. An *in vivo* study was performed in sheep where the composites degradation was evaluated using X-ray radiography.

2. Materials and methods

2.1. Material preparation

Iron powder (99.0 + % purity, 450 µm average particle size, Goodfellow, UK), HA and TCP were used to prepare Fe-bioceramic

* Corresponding author at: Faculty of Biosciences and Medical Engineering, Universiti Teknologi Malaysia, Skudai, Johor Bahru, 81310, Malaysia. Tel.: +60 7 5558493; fax: +60 7 5558515.

E-mail address: hendra.hermawan@biomedical.utm.my (H. Hermawan).

¹ Equal first author.

composites. Both HA and TCP nanopowders were synthesized using the microwave irradiation method as reported previously [22]. In brief, diammonium hydrogen phosphate $((\text{NH}_4)_2\text{HPO}_4, \text{QRec, China})$ solution was added dropwise into calcium nitrate tetrahydrate $(\text{Ca}(\text{NO}_3)_2 \cdot 4\text{H}_2\text{O}, \text{QRec, China})$ solution by maintaining Ca/P ratio at 1.67 (HA) and 1.5 (TCP). After the dripping was complete, the mixture was heated under microwave irradiation, filtered, dried at 80 °C, and sintered at 1000 °C for 1 h. The average particle size of the HA and TCP was about 70 ± 20 nm measured from field emission scanning electron microscope (FE-SEM) images ($n = 30$).

Samples of pure Fe and three different Fe-bioceramic composites were prepared by firstly mixing the starting powders at a nominal composition of (1) 100 wt% Fe (pure Fe); (2) Fe-5 wt% HA (Fe-HA); (3) Fe-5 wt% TCP (Fe-TCP); and (4) Fe-5 wt (60% HA:40% TCP) (Fe-BCP). Each mixture was uniaxially pressed under 13.8 MPa into pellets 12.67 mm in diameter. All pellets were sintered in a tube furnace under vacuum at 1100 °C (10 °C/min) and held for 1 h and then cooled to room temperature (10 °C/min).

The morphologies and elemental compositions of the samples were investigated by a scanning electron microscope (SEM, Hitachi TM3000, Japan) equipped with an energy dispersive X-ray spectrometer (EDS, Bruker, USA). Their phase identification was performed by using an X-ray diffractometer (XRD, Bruker, USA) with Cu-K α radiation operated at 40 kV, 40 mA, step size 0.04° and counting time 15 s/step in a 2θ range of 10–90°. The mechanical properties of the samples were determined by uniaxial compression testing according to ASTM E9-09 standard [23]. Six samples from each category were compressed using a universal testing machine (Instron 5982, USA) at a constant crosshead speed of 0.6 mm/min under 100 kN load cell.

2.2. Degradation tests

The degradation behavior of the Fe-bioceramic composite samples was studied by weight loss, potentiodynamic polarization and electrochemical impedance spectroscopy (EIS) measurements. All degradation tests were carried out in simulated body fluid (Kokubo's solution) which was prepared according to the method developed by Kokubo et al. [24]. For the weight loss (immersion) test, polished and ultrasonic cleaned samples were soaked in the Kokubo's solution (50 ml) at 37 °C in a water bath. After 2 weeks, the samples were removed, dried and then observed under SEM/EDS. Potentiodynamic polarization was performed using a potentiostat equipped with flat-cell apparatus (VersaSTAT 3, Princeton Applied Research, USA) in the Kokubo's solution at room temperature. The pure Fe and Fe-based composite samples served as the working, graphite as the counter and Ag/AgCl as the reference electrodes, respectively. The exposed surface area of the working electrodes was 0.502 cm². A scanning rate of 0.2 mV from –1 to –1.5 V and an open circuit potential (OCP) of –0.78 V were set up. Corrosion rate was calculated from corrosion current taken from polarization curves using Tafel extrapolation. The EIS was performed in the same solution for up to 2 h at room temperature. VersaStudio software (Princeton Applied Research, USA) was used for data acquisition at open circuit potential over a frequency range from 100 kHz down to 1 mHz using a peak-to-peak 10 mV sinusoidal perturbation.

2.3. In vitro cell viability test

Primary rat smooth muscle cells (RSMCs) were isolated and cultured from the intestine of an 8 week, 200 g Sprague–Dawley rat (Primate Research Centre, Bogor Agricultural University, Indonesia). The RSMCs were cultured in Dulbecco's modified Eagle's medium (DMEM) with 1 mg/ml glucose supplemented with 10% fetal bovine serum (Gibco, USA), 1% penicillin and 1% streptomycin (Invitrogen, USA) and were maintained at 37 °C and 5% CO₂. Cell viability tests were conducted by both direct and indirect methods. For the direct method, RSMCs were seeded in 96-well plates (2.5×10^3 cells/ml) for 24 h, and

then directly treated with samples (each $158 \pm 3 \times 10^{-4}$ g with surface area 8–10 mm²) at 5 different groups: pure-Fe, Fe-HA, Fe-TCP, Fe-BCP and non-treated group as control. Four replicates were used for each group in both methods. Weight change of the samples after treatment was recorded for corrosion rate measurement. For the indirect method, each sample was incubated in 1500 μ l medium at 37 °C with 5% CO₂, and then 500 μ l of the medium was collected without agitation at 7 and 14 days. The collected medium was then inserted into 96-well plates which were previously seeded with RSMCs (2.5×10^3 cells/ml) for 24 h. For both methods, after 48 h incubation, the medium was collected for MTT assay.

Ten microliters of 5 mg/ml MTT stock solution (Sigma Aldrich, USA) was applied to each well and then incubated for 4 h before the supernatants were aspirated. The purple formazan crystals in each well were dissolved in 100 μ l acidified ethanol and the absorbance was measured by using a spectrophotometer (BioRad, USA) at 595–655 nm. Results were shown in percentage of MTT reduction as compared to the non-treated group, presuming that this group was 100%. The collected medium from direct and indirect MTT assay was further analyzed for Fe and Ca concentrations using an atomic absorption spectrophotometer (AAS, AA-7000 Shimadzu, Japan) and for P concentration by molybdovanadate method using a UV spectrometer (UV 200R, V Scientific, USA) at 660 nm. The concentrations were analyzed by SPSS v.16.0 (SPSS Inc., Chicago, IL) using one-way ANOVA and post hoc Duncan test at the 95% confidence level. A p -value < 0.05 was considered to indicate statistical significance.

2.4. In vivo implantation test

Implant prototypes ($5 \times 2 \times 0.5$ mm³) were machined from each group of Fe-bioceramic samples. Another implant with the same dimension was prepared using SS316L material (one of the most common metallic materials for internal fixation) as a control. Five male sheep (Indonesian thin-tailed sheep, age between 10 and 12 months and body weight of 14–16 kg) were used with ethical clearance from the Bogor Agricultural University Care and Ethics Committee (ACUC #03-2012 IPB). The health status of the animals was checked prior to anesthesia where a standardized balanced anesthetic protocol was used. After 24 h of fasting, the animals received premedication (Atropine®, 0.06 mg/kg iv, Indofarm, Indonesia) and 10 min later induced and continuously maintained with general anesthesia (Ilium Xylazine®, 0.1 mg/kg iv, Troy Laboratories, Australia). General antibiotic (Novamox-G®, 1 ml/10 kg, Nova Laboratories, Malaysia) and topical spray antibiotic (Limoxin-25 Spray®, Interchemie Werken, Holland) were given every 2 days for 6 days to avoid postoperative infection. The sheep were placed in the left and right lateral recumbence on the operating table and a medial surgical approach to the bone was used.

The implants were inserted into flatten bone defects drilled below the radius periosteum membrane of radial forelegs on medio proximal region. Each sheep received one implant on each leg. The wound and skin were closed with suture (Vicryl®, polyglactin 910, 5/0 in size, Ethicon, USA) and bandaged with wound tape (Hypafix®, BSN Medical, Sweden). Implant degradation was analyzed using a non-invasive X-ray radiography method. The sheep were handled in the radiograph table where the latero-medial view radiography was obtained by a Diagnostic X-ray unit (VR 1020, MA Medical, Japan) at 3, 9, 14, 35, 50, and 70 days after implantation. Radiogram density was analyzed using a GD-1A Pencil Type Digital Densitometer (GammaTec NDT, South Africa) in X-ray illuminator.

3. Results and discussions

3.1. Material characterization and mechanical testing

Fig. 1 shows the microstructure of the sintered and polished surface of the pure-Fe and Fe based composites. It can be seen that all samples

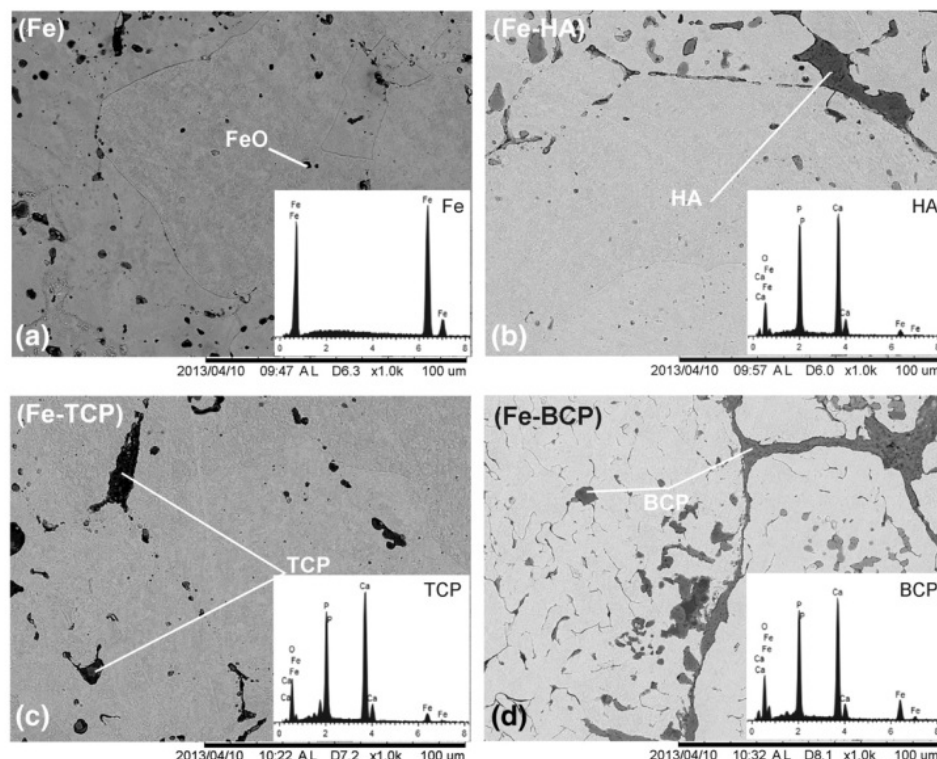


Fig. 1. SEM images and EDS spectra (inset) of (a) pure-Fe, (b) Fe-HA, (c) Fe-TCP, and (d) Fe-BCP.

were well sintered and the bioceramic phases with irregular shapes were distributed throughout Fe matrix. Few oxide phases were observed sparsely distributed in the pure-Fe sample, whereas in the Fe based composites, most of the bioceramic phases resided along Fe particle boundaries with a few of them dispersed within the Fe particles. The EDS results of the samples are shown in Table 1 which indicated the presence of Fe, P and Ca and their nominal composition. Fig. 2 presents XRD patterns of raw materials and the Fe-bioceramic composite samples. By comparing with the respective Joint Committee Powder Diffraction Standards (JCPDS) card numbers, the presence of HA and TCP in each Fe-HA and Fe-TCP sample was confirmed. The JCPDS card number for BCP was not applicable but its presence can be confirmed by the detected HA and TCP peaks in Fe-BCP sample. Therefore, these results provide evidence of the successful incorporation of HA, TCP and BCP into Fe.

The yield and compressive strength of the iron based composites were calculated from compression curves at strain $\varepsilon = 0.2\%$ and 35% , respectively (Table 2). It can be seen that the yield and compressive strengths decrease as the following: pure-Fe > Fe-HA > Fe-TCP > Fe-BCP.

A slight decrease was seen in the yield and compressive strengths of the Fe based composites compared to pure-Fe due to the inherent brittle nature of ceramics. The higher strength of Fe-HA compared to Fe-TCP

and Fe-BCP was believed to be attributable to a strong interface bonding between HA with Fe matrix and the superior compressive strength of HA compared to TCP [25]. Further investigation is needed to confirm this explanation; however it is not within the scope of this manuscript.

3.2. Degradation tests

Fig. 3 shows SEM images of the sample's surface after 2 weeks of immersion test showing a dark black pasty-like corrosion layer covering the surface. Some holes/pits were found beneath the corrosion layer after ultrasonic cleaning indicating localized corrosion. It was noticed that the chemical composition of the layer varied with the immersion time (Table 3). The Fe content decreased while Ca and P content increased with an increase in soaking time from 1 week to 2 weeks.

Weight changes of the samples during static immersion test for 1 and 2 weeks are shown in Fig. 4. It can be seen that the weight loss increases as the following: pure-Fe < Fe-HA < Fe-BCP < Fe-TCP. TCP is known to have higher solubility compared to HA in the body environment [21] which explains the obtained weight loss trend.

Fig. 5 shows typical potentiodynamic polarization curves of the samples. Corrosion potential of the Fe based composites was shifted to below that of the pure-Fe sample, while the corrosion current remained almost similar. As one of the primary constituents in HA and TCP, Ca is suspected to be the reason for the shift towards the active region similar to those that occur in Mg–Ca alloys [26]. The presence of PO_4^{3-} , Ca^{2+} and SO_4^{2-} ions in the Kokubo's solution could cause precipitation and consequently influence the shifting. The formation of Ca and P containing layer could behave as a passive layer, inhibiting current flow during the electrochemical corrosion tests.

Table 4 shows a comparison of corrosion rates calculated from potentiodynamic polarization, immersion test in Kokubo's solution and immersion test in contact with the cells. The trend of corrosion

Table 1

EDS results (area analysis) of the polished pure-Fe and Fe based composites samples in percentage of weight (wt%).

Element	Fe	Ca	P
Pure-Fe	100	–	–
Fe-HA	95	3	2
Fe-TCP	95	3	2
Fe-BCP	94	3	3

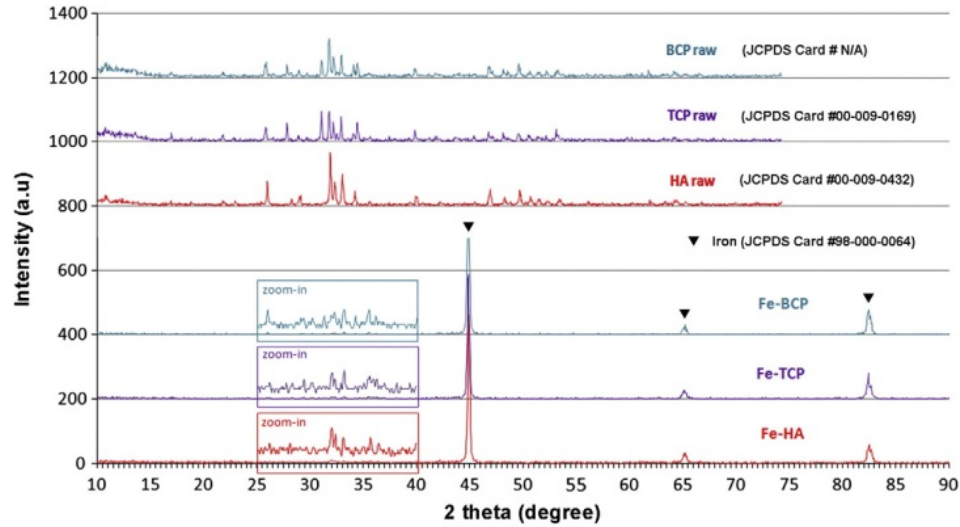


Fig. 2. XRD patterns of the raw bioceramics and the Fe based composites samples.

Table 2

Mechanical properties of the pure-Fe and Fe based composites samples.

Samples	0.2% offset yield strength (MPa)	Compressive strength (MPa)
Pure-Fe	354 ± 6	752 ± 13
Fe-HA	325 ± 5	717 ± 2
Fe-TCP	312 ± 1	708 ± 7
Fe-BCP	312 ± 2	696 ± 8

rate for samples tested with polarization and in contact with cells follows the order: pure-Fe > Fe-HA > Fe-BCP > Fe-TCP, while those immersed in Kokubo's solution follow a reverse order.

The difference in corrosion trend (Table 4) could be related to the time dependent effect. The short soaking period in potentiodynamic polarization (20 min) and in contact with cells (2 days) did not allow sufficient time for the dissolution of bioceramics similar to those

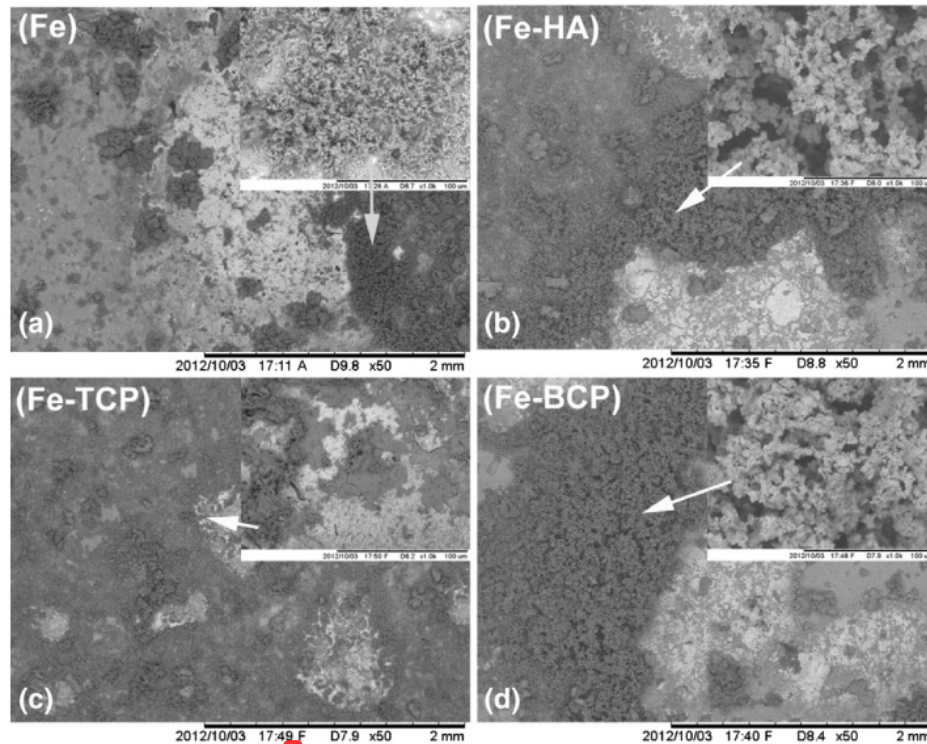


Fig. 3. SEM images of (a) pure-Fe, (b) Fe-HA, (c) Fe-TCP, and (d) Fe-BCP after immersion test for 2 weeks.

Table 3

EDS results (area analysis) of the surface of pure-Fe and Fe based composites samples after 1 and 2 weeks of immersion test (wt%).

Sample	Fe		O		Ca		P	
	W1	W2	W1	W2	W1	W2	W1	W2
Pure-Fe	50	32	33	45	7	6	11	13
Fe-HA	45	44	33	39	5	9	12	15
Fe-TCP	62	36	26	39	4	7	8	9
Fe-BCP	53	26	29	29	6	18	12	24

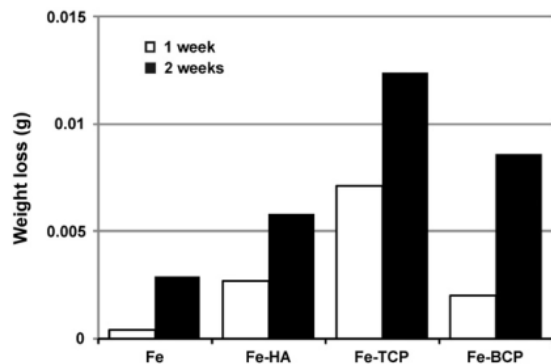
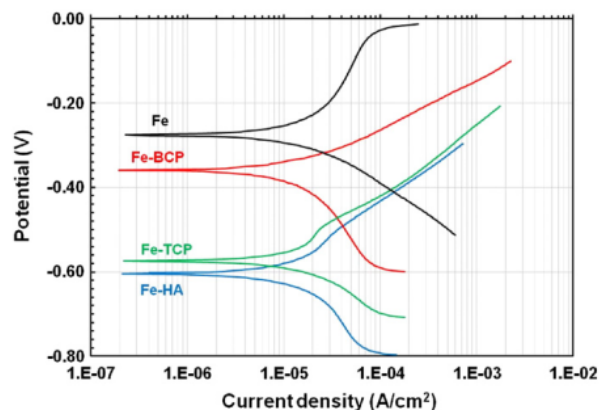
found immersed in the Kokubo's solution (2 weeks). A longer soaking period allowed the dissolution of bioceramics and the formation of a degradation layer. The effect of the degradation layer was then assessed by EIS measurement.

The EIS measurement provides basic information on the resistive and capacitive behavior at the interface of the samples and electrolyte (degradation layer). The inhibiting effect on the metal surfaces can also be predicted through this electrochemical measurement. Fig. 6 shows the Nyquist diagrams for the pure-Fe and the Fe based composite samples after 2 h exposure in the Kokubo's solution. Charge transfer resistance (R_{ct}) was determined from the Nyquist plot which corresponds to the measurement of electron transfer across the surface. The R_{ct} values were calculated as the difference in impedance at lower and higher frequencies [27]. The double layer capacitances (C_{dl}) that characterize charge separation between the Fe and electrolyte interface were also determined. Generally, the obtained impedance diagrams were not perfect semicircles and these results were attributable to frequency dispersion [28]. The plots in Fig. 6 show a larger impedance loop of Fe with the addition of 5% bioceramics compared to that of the Fe only. Larger impedance loops result in larger R_{ct} values, corresponding to the higher inhibiting corrosion effect [29].

Table 5 shows the values of impedance parameters for all the samples tested through the EIS measurement.

It can be seen in Table 5 that the inhibiting effect increased in the order of pure-Fe < Fe-HA < Fe-TCP < Fe-BCP. The inhibiting effect on the pure-Fe sample could be due to the formation of precipitation layer from PO_4^{3-} , Ca^{2+} and SO_4^{2-} ions in the Kokubo's solution. The higher inhibiting effect on the composite samples was due to the accumulation of P and Ca precipitate from the bioceramics matrix on the sample's surface. The weight loss results confirmed that the solubility of TCP was relatively higher than that of HA in body environment. This was the reason for the intense inhibiting effect of the composite samples as TCP molecules have a greater tendency to diffuse out from the ceramic matrix, thus forming the inhibiting passive layer.

Double layer capacitances (C_{dl}) were measured according to the equation $C_{dl} = (2\pi f_{max} R_{ct})^{-1}$ where f_{max} is the frequency at which the imaginary impedance component (Z_{im}) is maximum. The calculated

**Fig. 4.** Weight loss graphs of the pure-Fe and Fe based composites samples. Note: $n = 3$.**Fig. 5.** Potentiodynamic polarization graphs of the pure-Fe and Fe based composites samples.

C_{dl} values decreased following a trend: pure-Fe > Fe-HA > Fe-TCP > Fe-BCP, which is consistent with other reports related to EIS measurement of Fe [27,30]. The decrease of C_{dl} was due to the gradual replacement of water molecules by organic molecules (Ca and P) at the Fe/solution interface through the adsorption process. Fe-BCP and Fe-TCP have lower C_{dl} compared to that of Fe-HA due to TCP's higher dissolution than HA in body environment, which is consistent with the aforementioned R_{ct} result.

3.3. In vitro cell viability

Fig. 7 shows RSMCs viability and metal concentration measured from the MTT test samples.

Fe concentration was found higher in all direct contact method groups compared to those of indirect method. In the indirect method, the Fe concentration increased as the test was prolonged from 7 to 14 days. Table 6 details the elemental composition measured in the medium taken from MTT tests. Overall, the degradation trend for the indirect method follows that of the immersion test while the trend for the direct method was similar to that of potentiodynamic polarization. The direct method in Fig. 7 shows that the dissolution of bioceramics phases was inhibited by the cells' activity.

Compared to those in indirect contact, samples in direct contact with the cells induced higher Fe release to the culture medium regardless of the group (Fig. 7). The Fe-HA released more Fe followed by the Fe-TCP, pure-Fe and Fe-BCP groups (Table 6). Higher release of Fe correlates with lower cell viability as seen for the Fe-HA and Fe-TCP groups. A different trend was found in the direct method where the Fe-TCP released more Fe followed by the Fe-BCP, Fe-HA and pure-Fe groups (Table 6). The amount of Fe release does not correlate with cell viability confirming that indirect contact method involved no cellular activity during incubation as in the direct method. It was reported that Fe particles triggered different toxicity reactions based on the immediate environment such as biomolecules and physiological properties of culture

Table 4

Calculated corrosion rate of the pure-Fe and Fe based composites samples subjected to different methods.

Samples	Corrosion rate ($g/m^2 h$)		
	Potentiodynamic polarization (20 min)	Immersion in Kokubo's solution (2 weeks)	Immersion in contact with cells (2 days)
Pure-Fe	0.234	0.021	0.016
Fe-HA	0.199	0.042	0.013
Fe-BCP	0.192	0.062	0.011
Fe-TCP	0.181	0.090	0.010

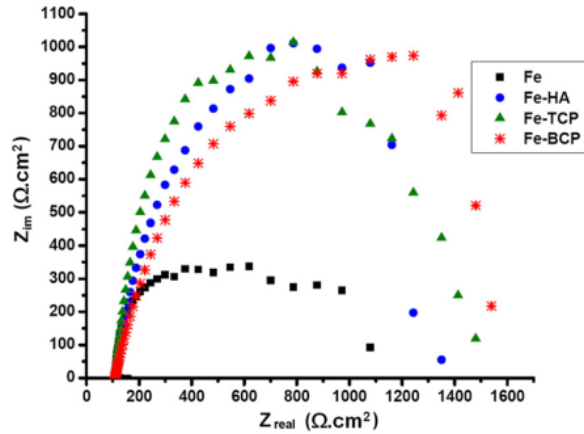


Fig. 6. Nyquist diagrams of the pure-Fe and Fe based composites samples.

Table 5
Impedance parameters of the pure-Fe and Fe based composites samples.

Samples	R_{ct} ($\Omega \text{ cm}^2$)	C_{dl} ($\mu\text{F/cm}^2$)
Pure-Fe	1000 ± 17	3183 ± 54
Fe-HA	1250 ± 4	1657 ± 5
Fe-TCP	1350 ± 21	785 ± 11
Fe-BCP	1500 ± 25	341 ± 5

Table 6

Fe, Ca, P concentration in RSMCs culture medium during MTT test.

Element	Groups (concentration in ppm)				
	Control	Pure-Fe	Fe-HA	Fe-TCP	Fe-BCP
<i>Direct (2 days)</i>					
Fe	na	722 ± 7^k	804 ± 5^m	754 ± 6^j	657 ± 5^l
Ca	na	282 ± 3^g	291 ± 1^s	287 ± 2^g	243 ± 1^d
P	na	324 ± 3^k	336 ± 7^k	329 ± 3^k	262 ± 7^i
<i>Indirect (7 days)</i>					
Fe	0 ^a	26 ± 1^b	149 ± 1^e	295 ± 4^i	140 ± 1^d
Ca	598 ± 14^k	455 ± 4^i	437 ± 2^h	459 ± 2^j	263 ± 4^e
P	160 ± 1^h	37 ± 1^a	76 ± 2^d	99 ± 1^f	94 ± 1^f
<i>Indirect (14 days)</i>					
Fe	0 ^a	126 ± 3^c	211 ± 3^g	277 ± 10^h	187 ± 5^f
Ca	598 ± 14^k	154 ± 4^a	210 ± 3^c	182 ± 5^b	184 ± 2^b
P	160 ± 1^h	33 ± 4^a	48 ± 1^b	63 ± 1^c	86 ± 1^e

Data shown as mean with standard deviation ($\bar{x} \pm \text{SD}$). The same letter in a different row and column shows the difference was not significant ($p > 0.05$). na = not analyzed.

medium [31]. Although Fe is essential element for mammals, including humans, Fe deregulation can induce cellular toxicity and develop cell degeneration through complex forms of Fe [32,33]. It has been reported that in the cells micro-environment, Fe ions caused cellular apoptosis, necrosis and apocrosis [34].

It is expected that at low concentration of Fe release (indirect method), the inhibition effect of Fe on cell growth was balanced by the

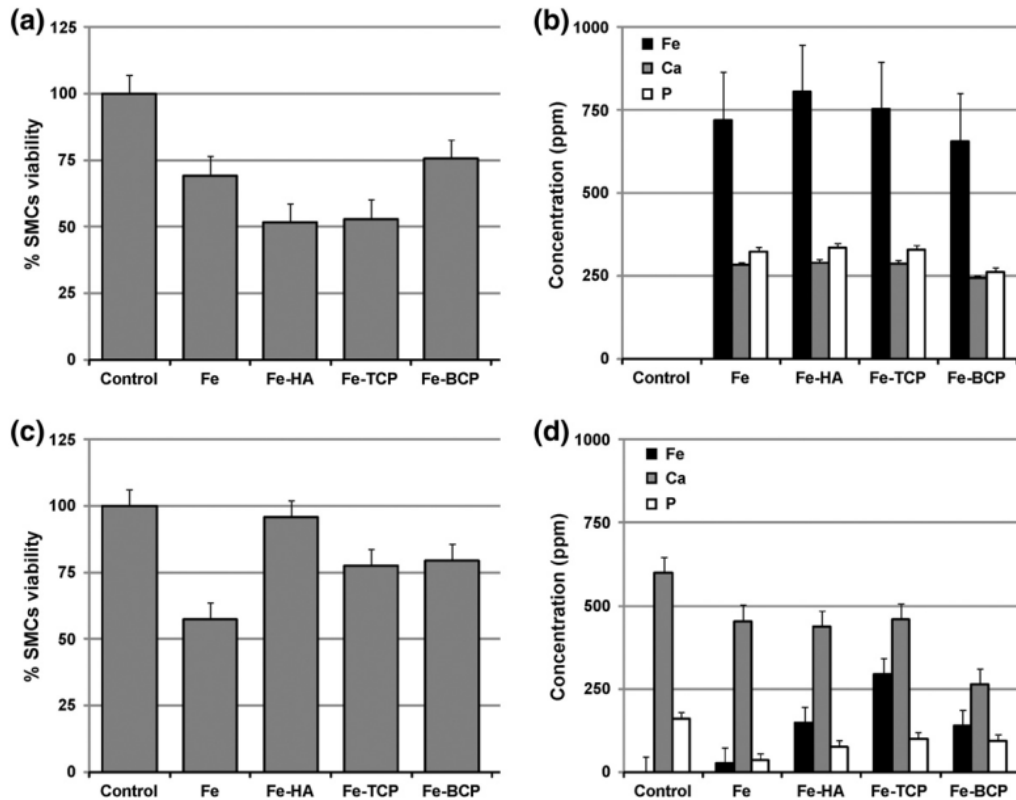


Fig. 7. Cell viability and metal concentration: (a, b) direct method, (c, d) indirect method.

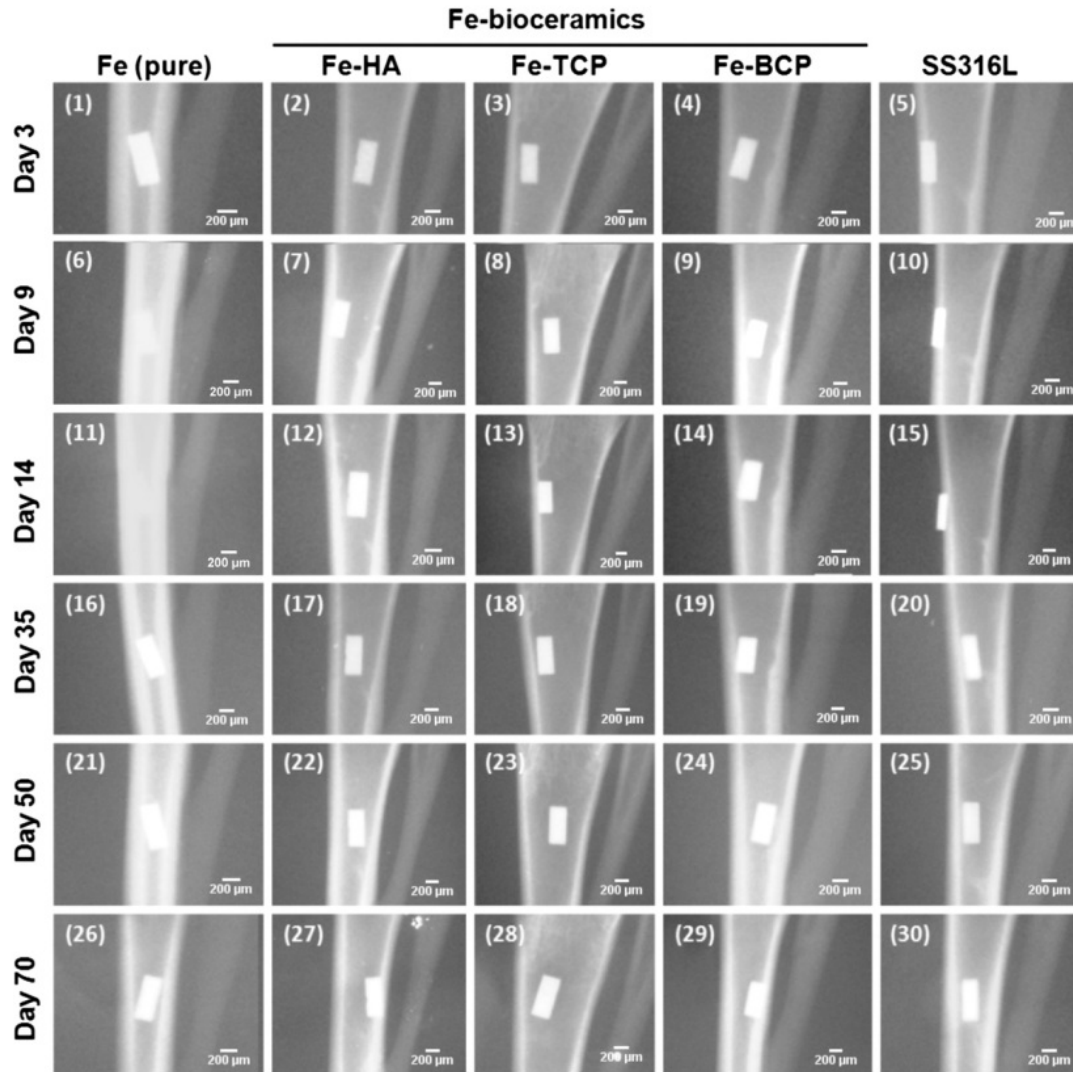


Fig. 8. X-ray radiograms of the pure-Fe, composites and SS316L samples at different implantation periods.

bioactive effect of the bioceramics (HA and TCP). However, the effect of Fe was dominant at higher concentrations (direct method). Direct contact of cells with degradable metals resulted into lower cell viability compared to indirect contact. During the direct contact test, the cells were subjected to a corrosion process where both anodic (Fe^{2+} release)

and cathodic (OH^- release) reactions occurred. For indirect contact, the cells interacted only with the degradation products with or without limited interaction with the degradation process itself. Further studies should be conducted to analyze the effect of complete degradation process and the composite's composition to the cells.

Table 7

Radiodensity analysis of the pure-Fe and Fe based composites implants.

Days	Implant type				
	Pure-Fe	Fe-HA	Fe-TCP	Fe-BCP	SS316L
3	67 ± 0^a	57 ± 1^j	62 ± 1^{lm}	61 ± 1^i	49 ± 1^f
9	68 ± 1^a	68 ± 1^{op}	68 ± 1^{op}	69 ± 1^q	60 ± 1^k
14	69 ± 0^{pq}	63 ± 1^m	64 ± 1^n	70 ± 1^q	54 ± 0^{hi}
35	50 ± 0^s	42 ± 1^b	42 ± 1^b	54 ± 0^{hi}	39 ± 1^a
50	50 ± 1^{fs}	53 ± 1^h	49 ± 1^{ef}	53 ± 1^h	39 ± 1^a
70	48 ± 1^e	55 ± 1^i	45 ± 1^d	61 ± 1^i	44 ± 1^c
Linear trendline	$y = -0.324x + 70$	$y = -0.102x + 58$	$y = -0.353x + 67$	$y = -0.121x + 67$	$y = -0.153x + 54$

Data shown as mean with standard deviation ($x \pm \text{SD}$). The same letter in a different row and column shows the difference was not significant ($p > 0.05$).

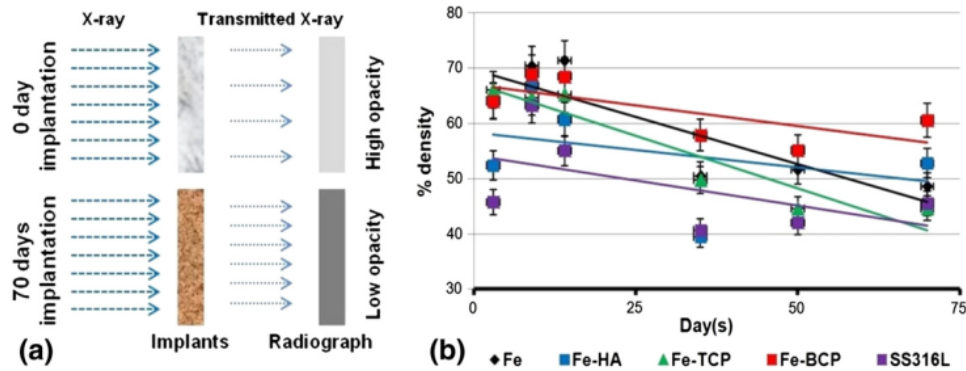


Fig. 9. Density analysis of X-ray radiograms: (a) illustration of the effect of degradation on radiodensity and (b) radiodensity change of the implants over implantation period.

3.4. X-ray radiography

Fig. 8 shows radiograms of pure-Fe, Fe-bioceramic composites and SS316L implants. Radiographic imaging is a non-invasive, simple yet powerful tool capable of identifying early changes or reactions of peri-implant tissues in the first week after implantation including clinical signs of bleeding, inflammation, and presence of exudates [35]. It can also provide useful information on implant morphology by analyzing radiographic density of the radiograms (radiodensity) [36–38]. The radiograms (Fig. 8) inform changes in implant density as indicated by the opacity of the images. Radiodensity was further quantitatively analyzed using a digital densitometer to avoid overlooking any small changes in the implants (Table 7).

Fig. 9a illustrates change on radiodensity as a result of the degradation process of the implants where degraded implants transmitted more X-ray than that of non- or less degraded implants. The increase of degradation attack correlates with lower material density and surface irregularities as confirmed by optical observation of the explanted implants (data not shown).

Fig. 9b shows that within 2 weeks after implantation, the radiodensity (opacity) of all implants increased, due mostly to the tissue healing process [39]. However, the radiodensity decreased as the implantation time increased due to implant degradation. The decrease was found to be higher for the Fe-TCP which is consistent with the *in vitro* immersion test (Fig. 4, Table 4). The increasing and decreasing trends were not applicable to the SS316L implant as degradation process did not occur except for the abrupt decrease from day 14 to day 35 which happens to all implants. It is also observed that the radiodensity of the Fe-HA and Fe-TCP increased from day 35 to day 50 but then decreased at day 70 (Table 7). Meanwhile, for the Fe-BCP implants the radiodensity showed a consistent increase after day 35. This trend is suspected to be related to the bioactive effect of bioceramics that promotes bone healing or bone formation around the Fe-bioceramic composite implants as also shown during the *in vitro* test (Fig. 7). It has been reported that the degradation of various bioceramic implants induced different kinds of bone formation [40,41].

4. Conclusion

In conclusion, the iron-based bioceramic (HA, TCP and BCP) composites were successfully prepared through the powder sintering process. The composites showed a slight decrease in yield and compressive strength compared to pure-Fe. Degradation of the Fe-bioceramic composites was slightly higher than the pure-Fe due to the incorporation of the degradable ceramics. The higher cell viability and cell proliferation of Fe-bioceramic composites demonstrate a positive effect of incorporating bioceramics into pure-Fe. X-ray radiographs confirmed the healing process and the degradation progress of all pure-Fe,

Fe-bioceramic composite and SS316L implants. The radiographs also indicate the superiority of the composite implants in terms of bone healing and formation.

Acknowledgements

The authors acknowledge the Malaysian Ministry of Higher Education and Universiti Teknologi Malaysia for the ERGS Grant RJ130000.7836.4L019, and Directorate General of Higher Education, Indonesian Ministry of Education and Culture for the Grant the 084/SP2H/PL/D/V/2013. The authors also thank Miss Nida Iqbal for providing us the HA and TCP powders and Miss Zulaika Miswan for her constructive comments on the language.

References

- [1] M. Peuster, P. Wohlsein, M. Bruggmann, M. Ehlerding, K. Seidler, C. Fink, H. Brauer, A. Fischer, G. Hausdorf, A novel approach to temporary stenting: degradable cardiovascular stents produced from corrodible metal—results 6–18 months after implantation into New Zealand white rabbits, *Heart* 86 (2001) 563–569.
- [2] H. Hermawan, *Biodegradable Metals: From Concept to Applications*, Springer, Heidelberg, Germany, 2012.
- [3] M. Peuster, C. Hesse, T. Schloo, C. Fink, P. Beerbaum, C.V. Schnakenburg, Long-term biocompatibility of a corrodible peripheral iron stent in the porcine descending aorta, *Biomaterials* 27 (2006) 4955–4962.
- [4] F. Witte, V. Kaese, H. Haferkamp, E. Switzer, A. Lindenberg-Meyer, C.J. Wirth, H. Windhagen, *In vivo* corrosion of four magnesium alloys and the associated bone response, *Biomaterials* 26 (2005) 3557–3563.
- [5] P. Peeters, M. Bosiers, J. Verbist, K. Deloese, B. Heublein, Preliminary results after application of absorbable metal stents in patients with critical limb ischemia, *J. Endovasc. Ther.* 12 (2005) 1–5.
- [6] B. Heublein, R. Rohde, V. Kaese, M. Niemeyer, W. Hartung, A. Haverich, Biocorrosion of magnesium alloys: A new principle in cardiovascular implant technology? *Heart* 89 (2003) 651–656.
- [7] R. Waksman, R. Pakala, R. Baffour, R. Seaborn, D. Hellings, F.O. Tio, Short-term effects of biocorrodible iron stents in porcine coronary arteries, *J. Interv. Cardiol.* 21 (2008) 15–20.
- [8] R.S. Stack, R.M. Califf, H.R. Phillips, D.B. Pryor, P.J. Quigley, R.P. Bauman, J.E. Tchong, J.C. Greenfield Jr., Interventional cardiac catheterization at Duke Medical Center, *Am. J. Cardiol.* 62 (1988) 3F–24F.
- [9] C. Di Mario, H. Griffiths, O. Goktekin, N. Peeters, J. Verbist, M. Bosiers, K. Deloese, B. Heublein, R. Rohde, V. Kaese, C. Illesley, R. Erbel, Drug-eluting bioabsorbable magnesium stent, *J. Interv. Cardiol.* 17 (2004) 391–395.
- [10] G. Song, S. Song, A possible biodegradable magnesium implant material, *Adv. Eng. Mater.* 9 (2007) 298–302.
- [11] E. Zhang, H. Chen, F. Shen, Biocorrosion properties and blood and cell compatibility of pure iron as a biodegradable biomaterial, *J. Mater. Sci. Mater. Med.* 21 (2010) 2151–2163.
- [12] S.F. Zhu, N. Huang, L. Xu, Y. Zhang, H. Liu, H. Sun, Y. Leng, Bio-compatibility of pure iron: *in vitro* assessment of degradation kinetics and cytotoxicity on endothelial cells, *Mater. Sci. Eng. C* 29 (2009) 1589–1592.
- [13] H. Hermawan, H. Alamdari, D. Mantovani, D. Dubé, Iron-manganese: New class of degradable metallic biomaterials prepared by powder metallurgy, *Powder Metall.* 51 (2008) 38–45.
- [14] M. Schinhammer, A.C. Hanzl, J.F. Löffler, P.J. Uggowitzer, Design strategy for biodegradable Fe-based alloys for medical applications, *Acta Biomater.* 6 (2010) 1705–1713.

- [15] M. Schinhammer, I. Gerber, A.C. Hänzli, P.J. Uggowitzer, On the cytocompatibility of biodegradable Fe-based alloys, *Mater. Sci. Eng. C* 33 (2013) 782–789.
- [16] H. Hermawan, D. Dube, D. Mantovani, Degradable metallic biomaterials: Design and development of Fe-Mn alloys for stent, *J. Biomed. Mater. Res. A* 93 (2010) 1–11.
- [17] B. Liu, Y.F. Zheng, Effects of alloying elements (Mn, Co, Al, W, Sn, B, C and S) on biodegradability and *in vitro* biocompatibility of pure iron, *Acta Biomater.* 7 (2011) 1407–1420.
- [18] C. Ohtsuki, M. Kamitakahara, T. Miyazaki, Bioactive ceramic-based materials with designed reactivity for bone tissue regeneration, *J. R. Soc. Interface.* 6 (2009) S349–S360.
- [19] H. Kawahara, Bioceramics for hard tissue replacements, *Clin. Mater.* 2 (1987) 181–206.
- [20] K.Y. Renkema, R.T. Alexander, R.J. Bindels, J.G. Hoenderop, Calcium and phosphate homeostasis: Concerted interplay of new regulators, *Ann. Med.* 40 (2008) 82–91.
- [21] Å. Bengtsson, A. Shchukarev, P. Persson, S. Sjöberg, A solubility and surface complexation study of a non-stoichiometric hydroxyapatite, *Geochim. Cosmochim. Acta* 73 (2009) 257–267.
- [22] N. Iqbal, M.R. Abdul Kadir, N.A.N. Nik Malek, N. Humaimi Mahmood, M. Raman Murali, T. Kamarul, Rapid microwave assisted synthesis and characterization of nanosized silver-doped hydroxyapatite with antibacterial properties, *Mater. Lett.* 89 (2012) 118–122.
- [23] ASTM E9: Standard Test Methods of Compression Testing of Metallic Materials at Room Temperature, ASTM International, West Conshohocken, 2009.
- [24] T. Kokubo, H. Takadama, How useful is SBF in predicting *in vivo* bone bioactivity? *Biomaterials* 27 (2006) 2907–2915.
- [25] D.E. Grenoble, J.L. Katz, K.L. Dunn, R.S. Gilmore, K.L. Murty, The elastic properties of hard tissues and apatites, *J. Biomed. Mater. Res.* 6 (1972) 221–233.
- [26] M.B. Kannan, R.K.S. Raman, *In vitro* degradation and mechanical integrity of calcium-containing magnesium alloys in modified-simulated body fluid, *Biomaterials* 29 (2008) 2306–2314.
- [27] F. Bentiss, M. Traisnel, M. Lagrenée, The substituted 1,3,4-oxadiazoles: a new class of corrosion inhibitors of mild steel in acidic media, *Corros. Sci.* 42 (2000) 127–146.
- [28] F. Mansfeld, M.W. Kending, S. Tsai, Evaluation of corrosion behavior of coated metals with AC impedance measurements, *Corrosion* 38 (1982) 478–485.
- [29] M. Lebrini, F. Bentiss, N. Chihib, C. Jama, J.P. Hornez, M. Lagrenée, Polyphosphate derivatives of guanidine and urea copolymer: Inhibiting corrosion effect of Amco iron in acid solution and antibacterial activity, *Corros. Sci.* 50 (2008) 2914–2918.
- [30] H. Amar, J. Benzakour, A. Derja, D. Villemain, B. Moreau, T. Braisaz, Piperidin-1-yl-phosphonic acid and (4-phosphono-piperazin-1-yl) phosphonic acid: A new class of iron corrosion inhibitors in sodium chloride 3% media, *Appl. Surf. Sci.* 252 (2006) 6162–6172.
- [31] C.R. Keenan, D.L. Sedlak, Factors affecting the yield of oxidants from the reaction of nanoparticulate zero-valent iron and oxygen, *Environ. Sci. Technol.* 42 (2008) 1262–1267.
- [32] C.R. Keenan, R. Goth-Goldstein, D. Lucas, D.L. Sedlak, Oxidative stress induced by zero-valent iron nanoparticles and Fe(II) in human bronchial epithelial cells, *Environ. Sci. Technol.* 43 (2009) 4555–4560.
- [33] C.M. Nday, G. Malollari, S. Petanidis, A. Salifoglou, *In vitro* neurotoxic Fe(III) and Fe(III)-chelator activities in rat hippocampal cultures. From neurotoxicity to neuroprotection prospects, *J. Inorg. Biochem.* 117 (2012) 342–350.
- [34] S.D. Ray, G.B. Corcoran, Cell Death and Apoptosis, General, Applied and Systems Toxicology, John Wiley & Sons, Ltd., 2009.
- [35] N. Pauleto, B.J. Lahiffe, J.N. Walton, Complications associated with excess cement around crowns on osseointegrated implants: A clinical report, *Int. J. Oral Maxillofac. Implants* 14 (1999) 865–868.
- [36] R.B. Fonseca, C.A. Branco, P.V. Soares, L. Correr-Sobrinho, F. Haiter-Neto, A.J. Fernandes-Neto, C.J. Soares, Radiodensity of base, liner and luting dental materials, *Clin. Oral Investig.* 10 (2006) 114–118.
- [37] K.L. Devito, A.J. Ortega, F. Haiter-Neto, Radiopacity of calcium hydroxide cement compared with human tooth structure, *J. Appl. Oral Sci.* 12 (2004) 290–293.
- [38] S. Gu, B.J. Rasimick, A.S. Deutsch, B.L. Musikant, Radiopacity of dental materials using a digital X-ray system, *Dent. Mater.* 22 (2006) 765–770.
- [39] C. Wadhvani, T. Hess, T. Faber, A. Piñeyro, C.S. Chen, A descriptive study of the radiographic density of implant restorative cements, *J. Prosthet. Dent.* 103 (2010) 295–302.
- [40] M. Bashoor-Zadeh, G. Baroud, M. Böhner, Simulation of the *in vivo* resorption rate of b-tricalcium phosphate bone graft substitutes implanted in a sheep model, *Biomaterials* 32 (2011) 6362–6373.
- [41] U. Ripamonti, L.C. Roden, L.F. Renton, Osteoinductive hydroxyapatite-coated titanium implants, *Biomaterials* 33 (2012) 3813–3823.

In vitro and in vivo degradation evaluation of novel iron-bioceramic composites

ORIGINALITY REPORT

14%

SIMILARITY INDEX

8%

INTERNET SOURCES

11%

PUBLICATIONS

0%

STUDENT PAPERS

MATCH ALL SOURCES (ONLY SELECTED SOURCE PRINTED)

8%

★ Mokhamad F. Ulum, Ahmad K. Nasution, Abdul H. Yusop, Andril Arafat et al. " Evidences of bioactivity of Fe-bioceramic composites for temporary bone implants ", Journal of Biomedical Materials Research Part B: Applied Biomaterials, 2015

Publication

Exclude quotes On

Exclude bibliography On

Exclude matches < 3%